Supporting Information

Pore-coordination sphere facilitated ratiometric fluorescent detection of organic amines in a substitutional metal–organic matrix

Kai Xing,[*a] Xiao-Yuan Liu,[*b] Cheng-Shan Ji,[c] and Jing Li[*db]

[a] Department of Chemistry, College of Basic Medicine, Third Military Medical University (Army Medical University), Chongqing, 400038, P.R. China

[b] Hoffmann Institute of Advanced Materials, Shenzhen Polytechnic University, 7098 Liuxian Blvd, Nanshan District, Shenzhen, 518055, P.R. China

[c] MIIT Key Laboratory of Critical Materials Technology for New Energy Conversion and Storage, School of Chemistry and Chemical Engineering, Harbin Institute of Technology, Harbin, 150001, P. R. China

[d] Department of Chemistry and Chemical Biology, Rutgers University, 123 Bevier Road, Piscataway, New Jersey, 08854, United States

Contents

Section 1. Materials and Methods 3

Section 2. Structural Information.....4

Section 3. General Characterization.....5

Section 4. Fluorescent Measurements 8

References 20

Section 1. Materials and Methods

Chemical stability

10 mg finely ground HIAM-3001, HIAM-3002 and HIAM-3001-PNT-25% powders were immersed in 5 mL of deionized water for 72 h; then the MOF powders were centrifuged and used to measure the PXRD patterns.

Computational Methods

The geometries of PBT and PNT without and with methylamine were performed with Gaussian09 program.[1] To the ground state, the density functional theory (DFT) were applied using range-separated CAM-B3LYP functional together with 6-31g+(d,p) basis set in the conductor-like polarizable continuum model (CPCM) after considering the solvent effects of water (ε = 78.36). Accordingly, the geometries of excited states were optimized using the time-dependent density functional theory (TDDFT) with CAM-B3LYP functional and 6-31g+(d,p) basis set.

Section 2. Structural Information

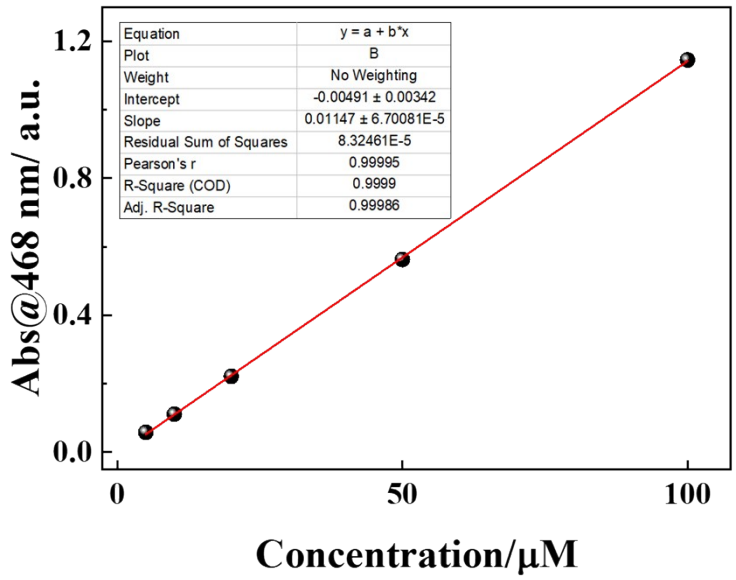

Fig. S1 Standard curve for quantification of PNT by UV-Vis spectra.

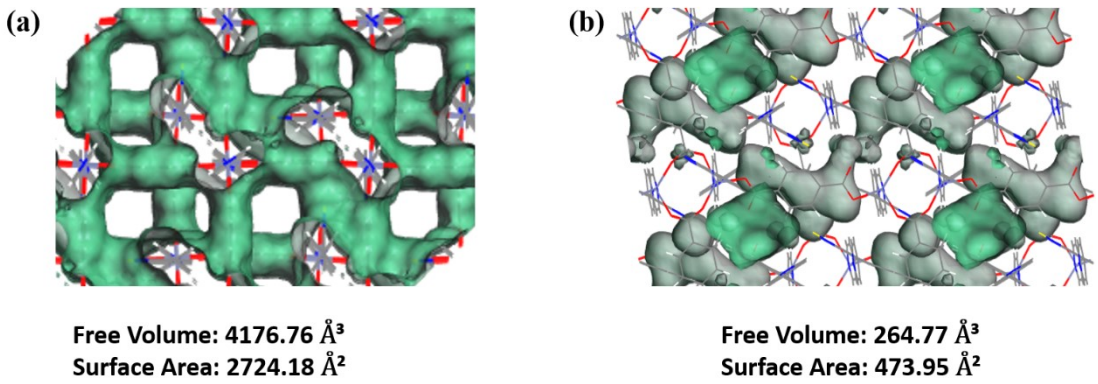

Fig. S2 (a) Solvent accessible void space of **HIAM-3001**; (b) Solvent accessible void space of **HIAM-3002** (gray: outer site of the pore and green: inner site of the pore).

Section 3. General Characterization

Thermogravimetric Analysis

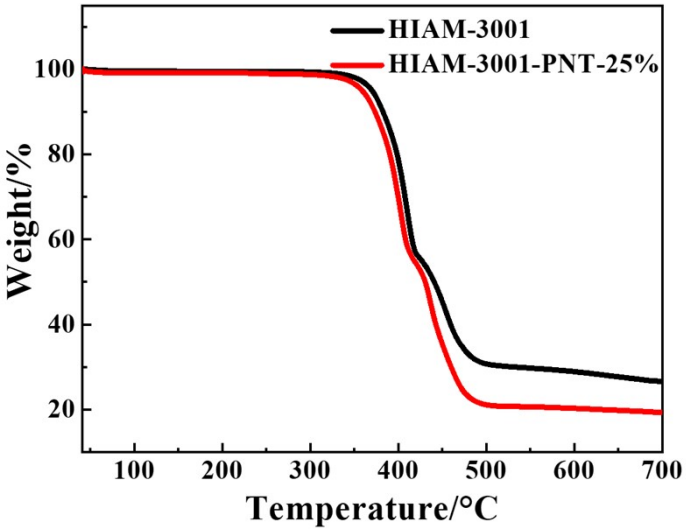

Fig. S3 TGA curves of **HIAM-3001** and **HIAM-3001-PNT-25%**.

Powder X-ray Diffraction Patterns

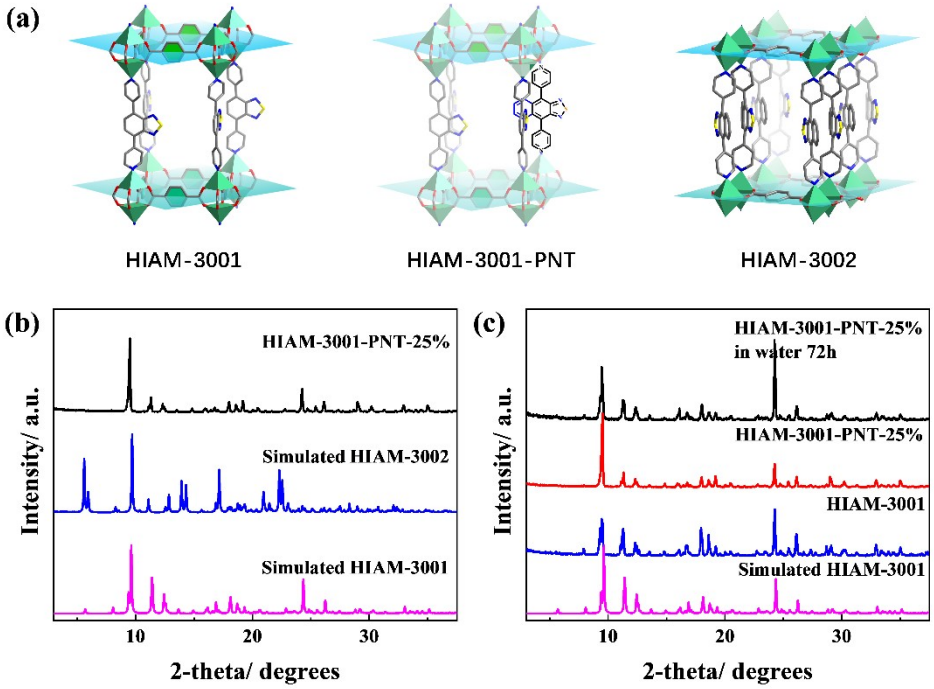

Fig. S4 (a) Scheme of PNT ligand doping in pristine **HIAM-3001** matrix; (b) PXRD patterns of the as-synthesized **HIAM-3001-PNT-25%**, the simulated **HIAM-3001** and **HIAM-3002**; (c) PXRD patterns of the as-synthesized **HIAM-3001-PNT-25%** and **HIAM-3001-PNT-25%** after treatment in water for 72 h, in comparison with those of simulated and as-synthesized **HIAM-3001**.

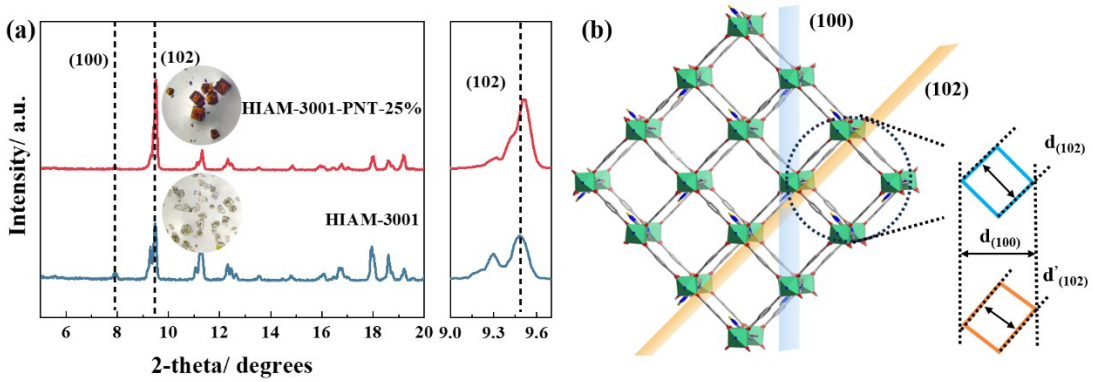

Fig. S5 (a) PXRD profiles of **HIAM-3001** and **HIAM-3001-PNT-25%** (inset: crystal pictures); (b) schematic illustration of the framework change of **HIAM-3001** after ligand doping.

Hirshfeld surfaces analysis

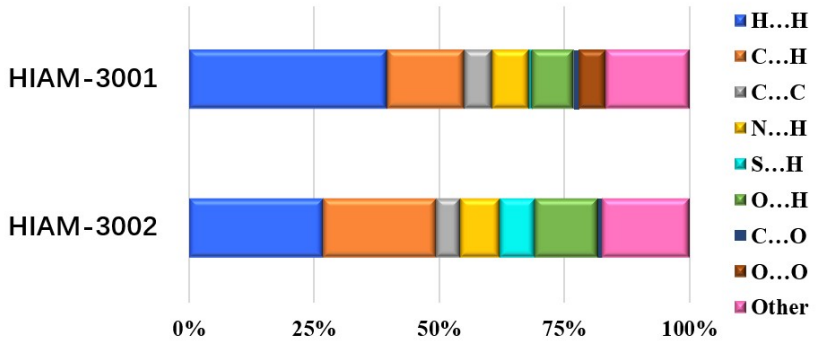

Fig. S6 The bar chat of relative contributions for **HIAM-3001** and **HIAM-3002** to the Hirshfeld surface area for the various close intermolecular contacts.

Section 4. Fluorescent Measurements

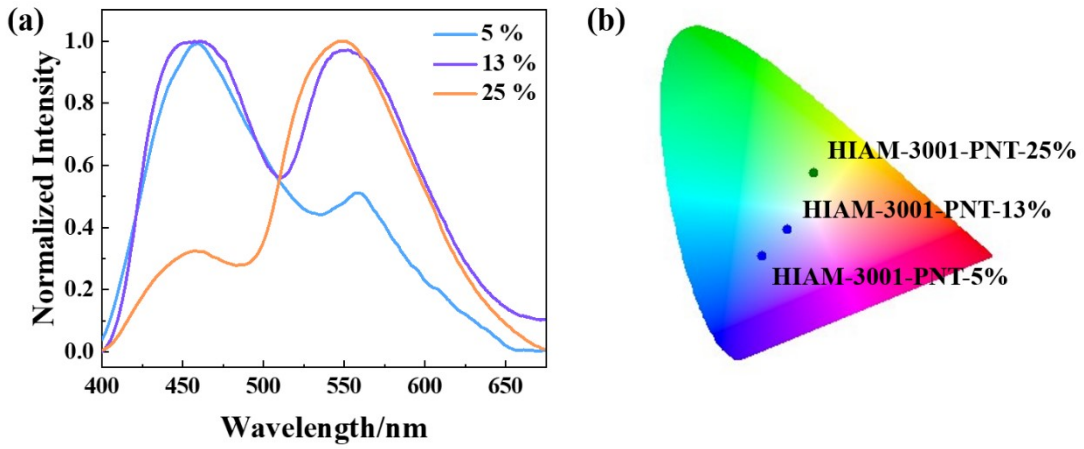

Fig. S7 Emission spectra of fluorescence mapping of **HIAM-3001-x%** with different ratios.

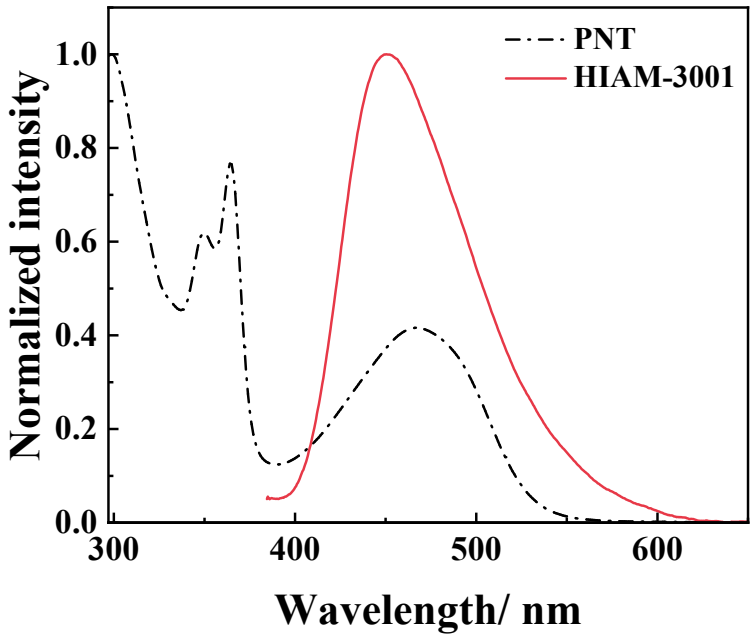

Fig. S8 Emission spectra of **HIAM-3001** (solid line) and UV absorbance of **PNT** (dashed dot line).

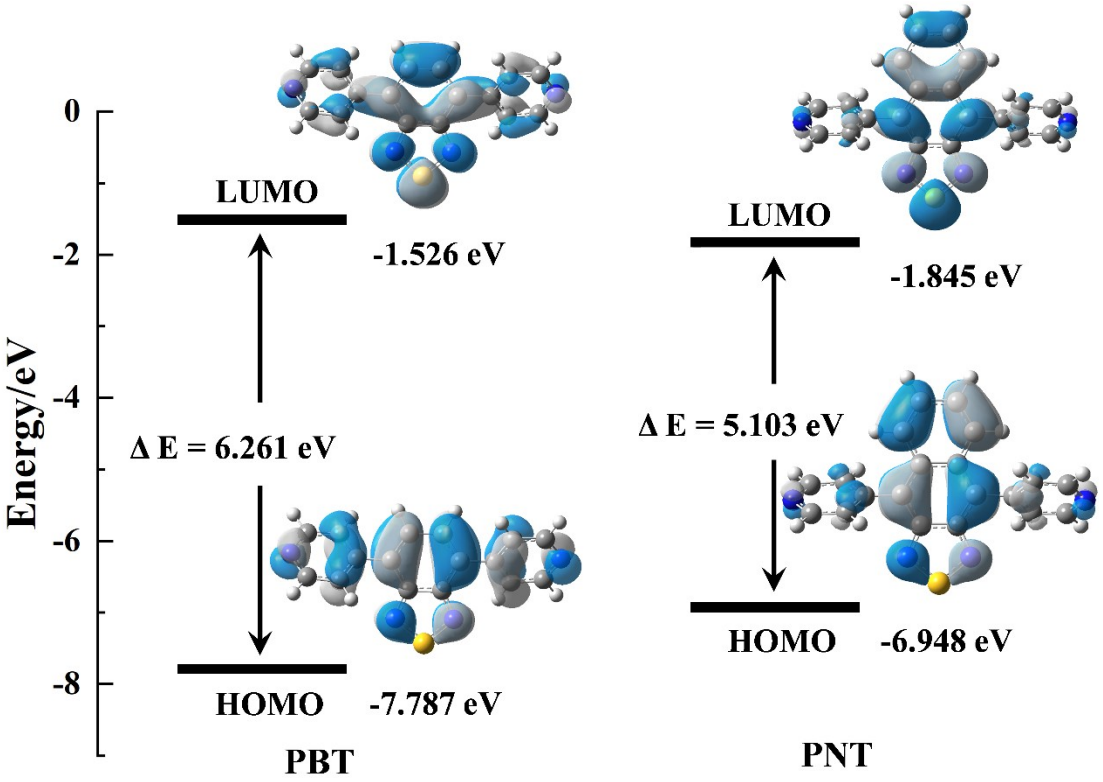

Fig. S9 Calculated HOMO and LUMO orbitals of **PBT** and **PNT** and their HOMO-LUMO energy gap, plotted with an isovalue of 0.04.

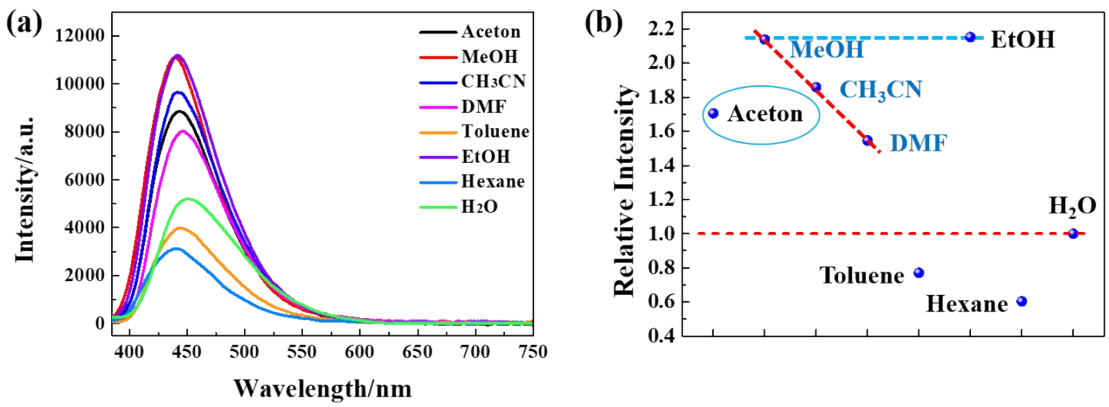

Fig. S10 (a) The emission, (b) relative intensity of **HIAM-3001** in different solvents.

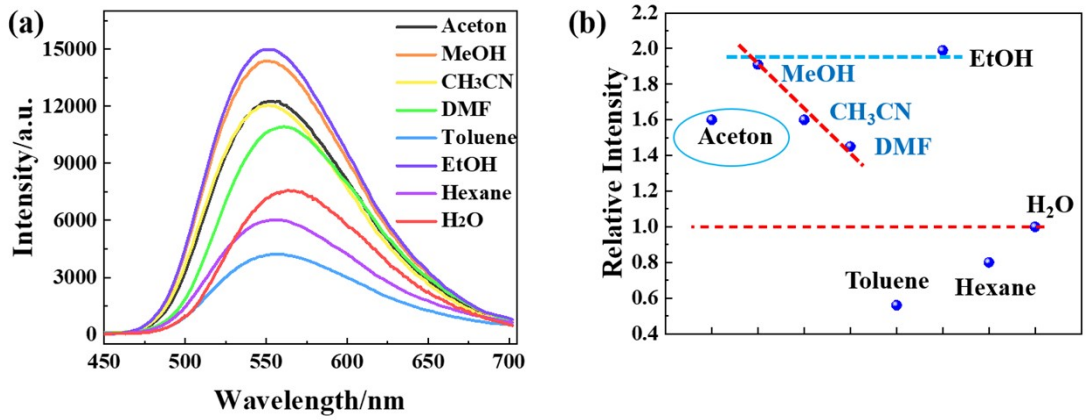

Fig. S11 (a) The emission, (b) relative intensity of **HIAM-3002** in different solvents.

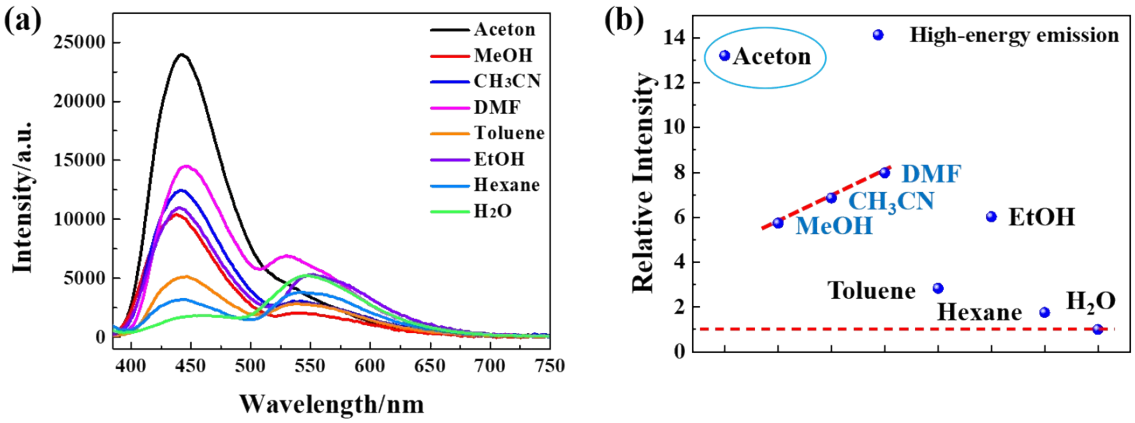

Fig. S12 (a) The emission, (b) relative intensity of **HIAM-3001-PNT-25%** in different solvents.

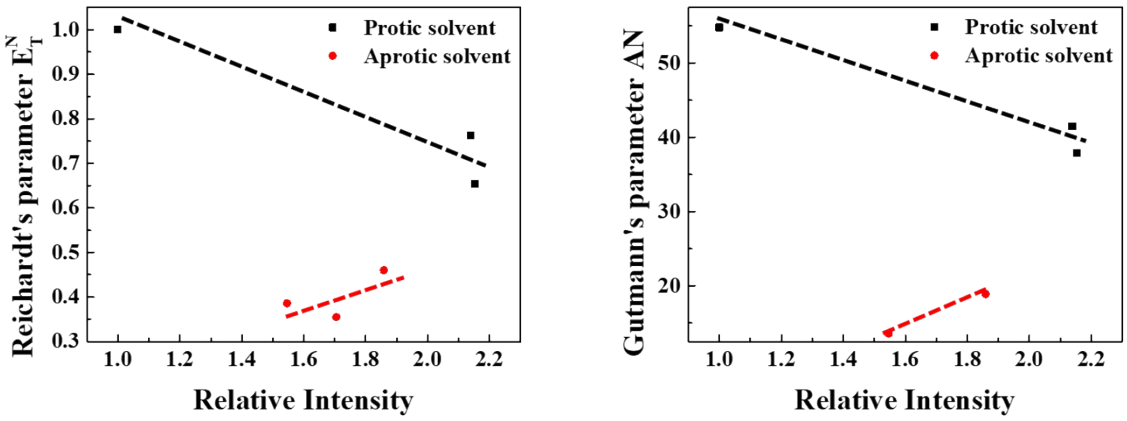

Fig. S13 The relation between relative intensity and corresponding different solvent parameters for various solvents with different protic property for **HIAM-3001**.

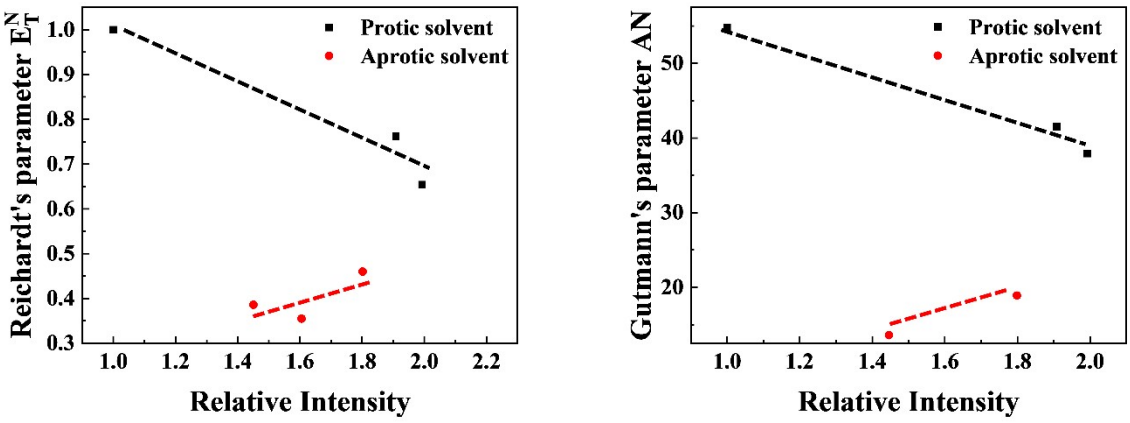

Fig. S14 The relation between relative intensity and corresponding different solvent parameters for various solvents with different protic property for **HIAM-3002**.

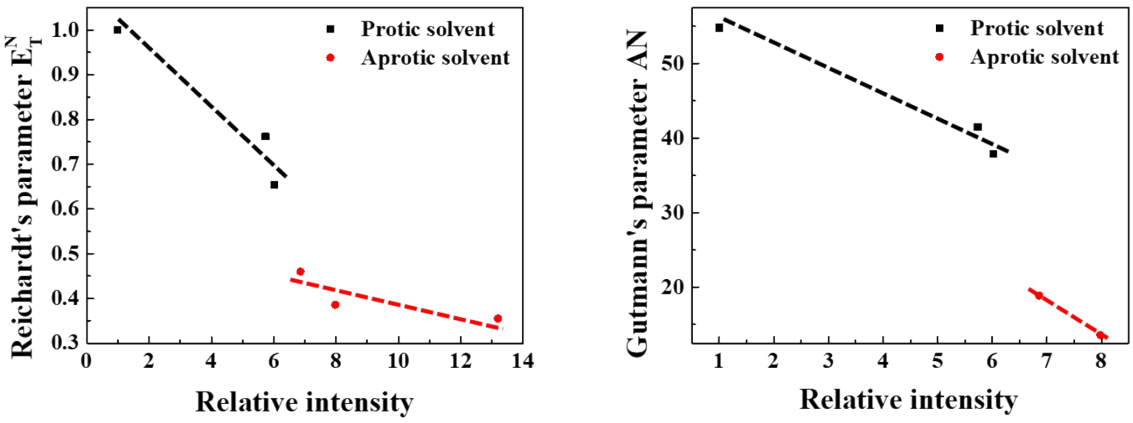

Fig. S15 The relation between relative intensity and corresponding different solvent parameters for various solvents with different protic property for **HIAM-3001-PNT-25%**.

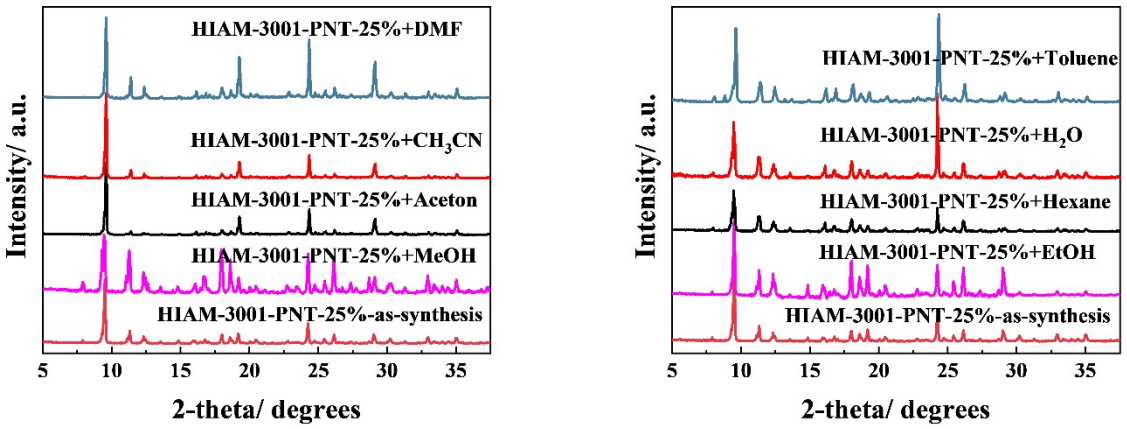

Fig. S16 The PXRD profiles of **HIAM-3001-PNT-25%** after immersing in different solvents for 72 h.

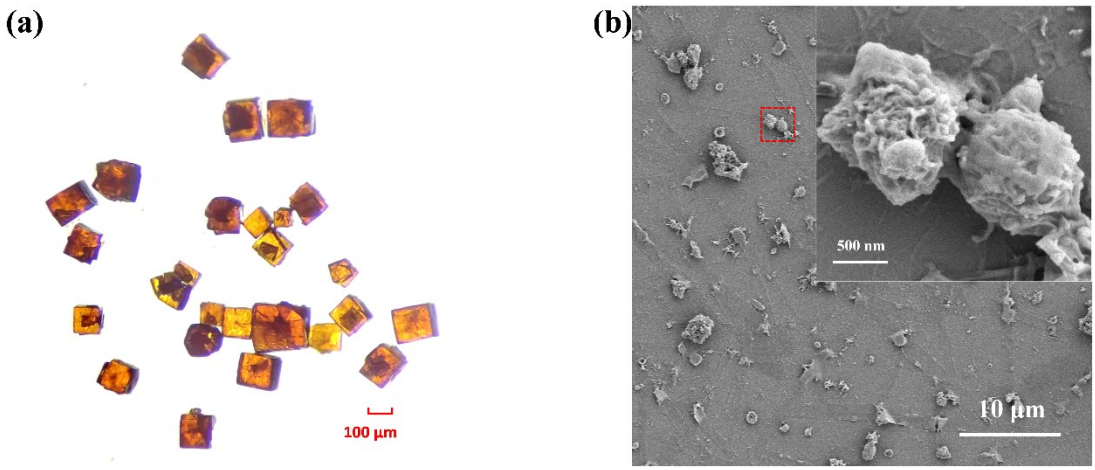

Fig. S17 (a) Optical crystal photos of as-synthesized **HIAM-3001-PNT-25%**; (b) SEM image of **HIAM-3001-PNT-25%** after grinding.

Table S1 Solvent dependent luminescence properties of **HIAM-3001**, **HIAM-3002** and **HIAM-3001-PNT-25%**.

Solvent	Solvent parameters		Luminescent property					
	Reichardt's parameters	Gutmann's parameters	HIAM-3001		HIAM-3002		HIAM-3001-PNT-25%	
	E_T^N	AN	Relative intensity	CIE X/ CIE Y	Relative intensity	CIE X/ CIE Y	Relative intensity	CIE X/ CIE Y
Acetonitrile	0.460	18.9	1.86	(0.15,0.11)	1.80	(0.41,0.54)	6.86	(0.20,0.17)
Acetone	0.355	-	1.71	(0.15,0.10)	1.60	(0.42,0.55)	13.19	(0.18,0.14)
MeOH	0.762	41.5	2.14	(0.15,0.09)	1.91	(0.41,0.56)	5.73	(0.20,0.15)
EtOH	0.654	37.9	2.15	(0.15,0.10)	1.99	(0.41,0.55)	6.02	(0.26,0.24)
DMF	0.386	13.6	1.55	(0.16,0.12)	1.45	(0.44,0.54)	7.98	(0.22,0.24)
H_2O	1	54.8	1.0	(0.16,0.15)	1.0	(0.46,0.53)	1.0	(0.34,0.45)
Toluene			0.77	(0.15,0.11)	0.56	(0.43,0.54)	2.83	(0.25,0.26)
n-Hexane			0.60	(0.16,0.10)	0.80	(0.43,0.55)	1.75	(0.30,0.36)

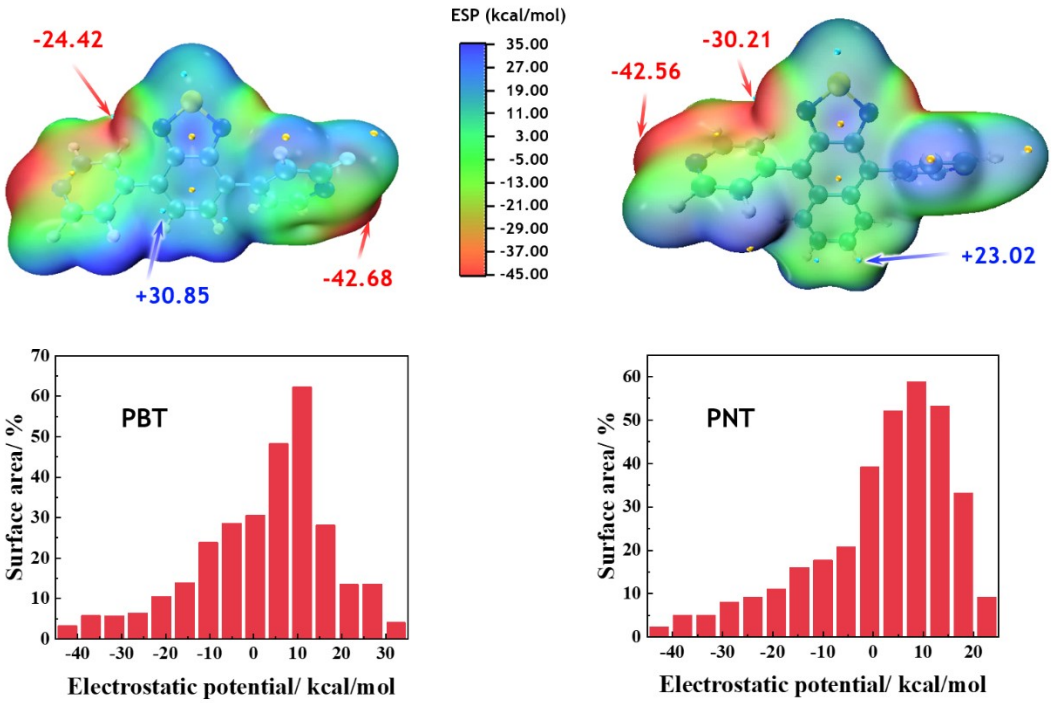

Fig. S18 ESP-mapped molecular *vdW* surface and Electrostatic potential distribution of PBT (left) and PNT (right). (Significant surface local minima and maxima of ESP are represented as orange and azure spheres, respectively).

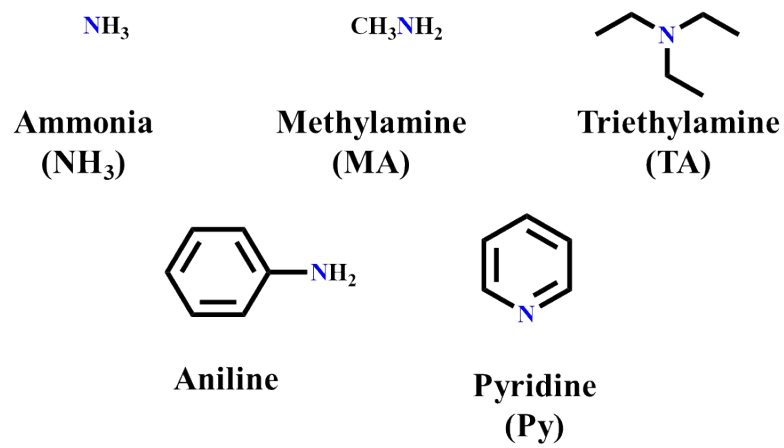

Scheme S1 Structures of the selected organic amine analytes.

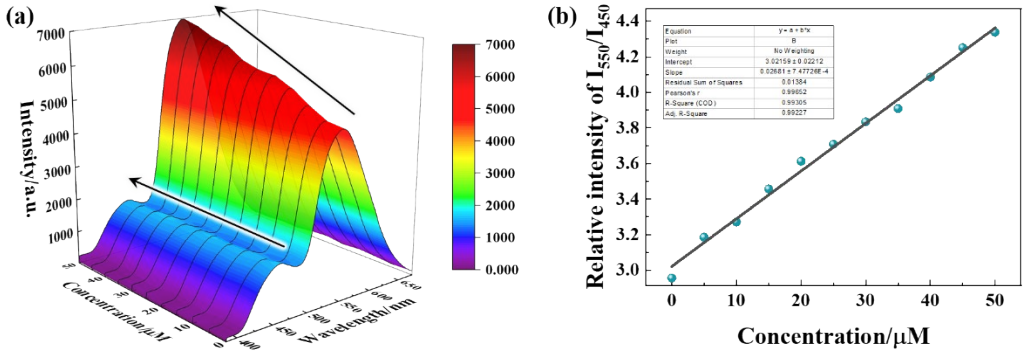

Fig. S19 (a) Effect on the fluorescence of **HIAM-3001-PNT-25%** dispersed in water upon the incremental addition of ammonia solution; (b) linear fit for the estimation of detection limit.

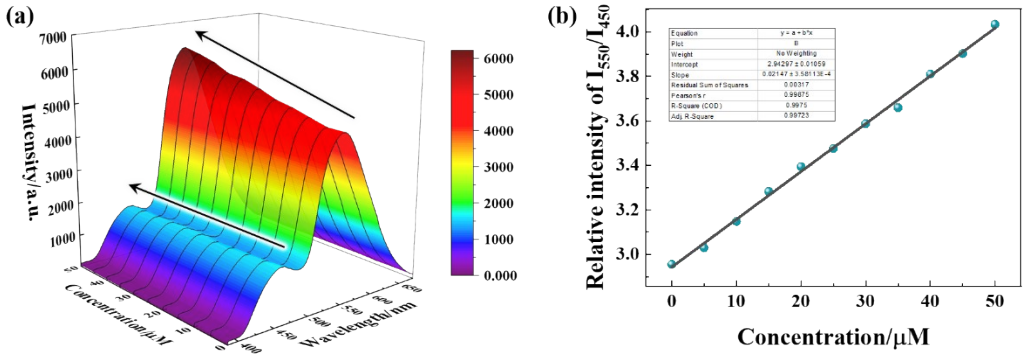

Fig. S20 (a) Effect on the fluorescent spectra of **HIAM-3001-PNT-25%** dispersed in water upon the incremental addition of methylamine; (b) linear fit for the estimation of detection limit.

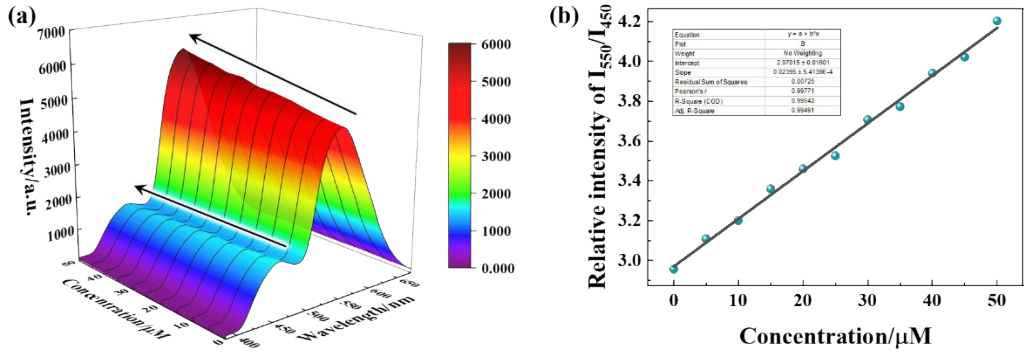

Fig. S21 (a) Effect on the fluorescence of **HIAM-3001-PNT-25%** dispersed in water upon the incremental addition of triethylamine; (b) linear fit for the estimation of detection limit.

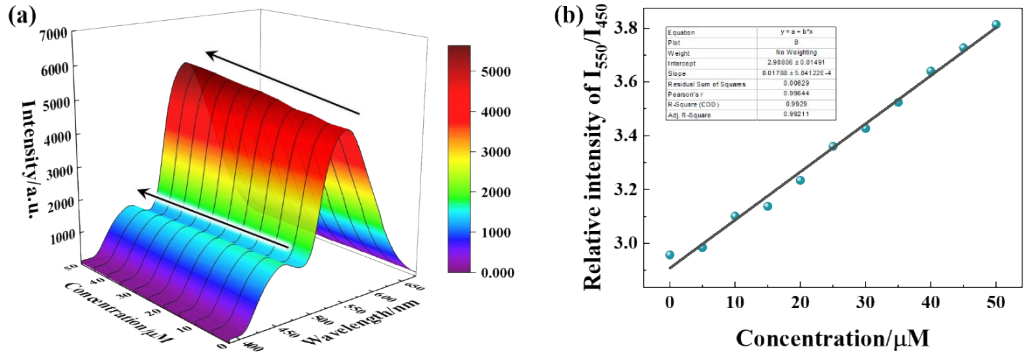

Fig. S22 (a) Effect on the fluorescence of **HIAM-3001-PNT-25%** dispersed in water upon the incremental addition of cadaverine; (b) linear fit for the estimation of detection limit.

Table S2 The limit of detection of selected analytes.

Analytes	The limit of detection (LOD)
Ammonia (NH_3)	0.299 ppm
Methylamine (MA)	0.681 ppm
Triethylamine (TA)	1.990 ppm
Cadaverine (PDA)	2.691 ppm

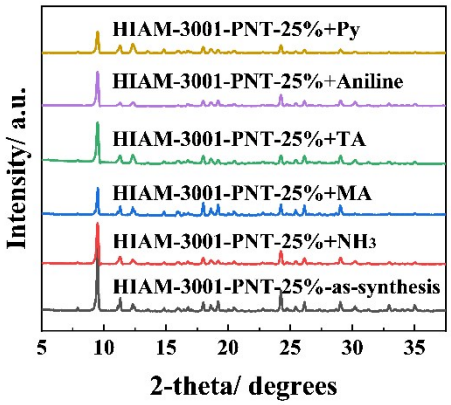

Fig. S23 PXRD profiles of **HIAM-3001-PNT-25%** before and after fluorescent sensing.

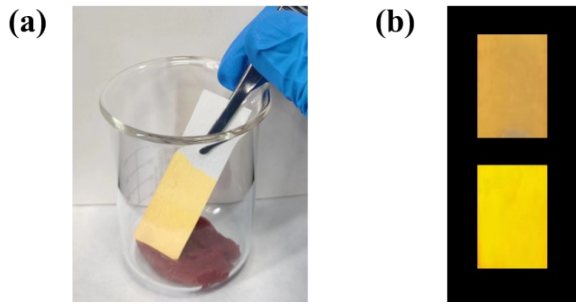

Fig. S24 (a) Optical image of **HIAM-3001-PNT-25%** coated filter paper strip in the presence of spoiled beef at room temperature; (b) images of **HIAM-3001-PNT-25%** coated filter paper before (top) and after (bottom) presenting in the spoiled beef.

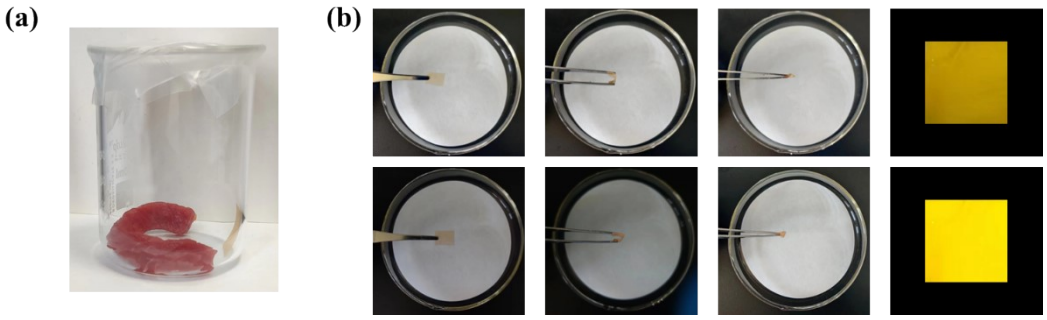

Fig. S25 (a) Membrane exposure to the vapours from spoiled beef; (b) flexible membranes of **HIAM-3001-PNT-25%** before (top) and after (bottom) exposure to the vapours from spoiled beef.

References

1 M. J. Frisch and e. al., *Gaussian 09, rev. D.01; Gaussian Inc.: Wallingford, CT*, 2013.